Tribology International 164 (2021) 107221

Contents lists available at ScienceDirect

Tribology International

journal homepage: www.elsevier.com/locate/triboint

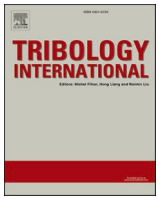

Oil property sensing array based on a general regression neural network

Dian Jiao, Aaron Urban, Xiaoliang Zhu, Jiang Zhe *

Department of Mechanical Engineering, The University of Akron, Akron, OH 44325, United States

ARTICLE INFO

Keywords:
Lubrication oil
Monitoring
Measurement
Neural network

ABSTRACT

Online monitoring of multiple lubricant properties is critical in maintaining and extending the health of high-speed rotating and reciprocating machinery used in many of the nation's key industries including aerospace, manufacturing, and energy. There have been many efforts on the development of sensors focused on measuring specific chemical/physical properties of lubricant oil. One long-standing challenge for these property sensors is the overlapping output problem (cross-sensitivity), meaning they cannot provide accurate measurements. Here we demonstrated a capacitive oil property sensor array based on a new general regression neural network (GRNN) for measuring acid, base, and water content in lubricant oil. Results showed that the GRNN can pinpoint individual oil properties from the overlapped sensor array's responses with high accuracy and speed.

1. Introduction

The productivity and lifespan of machinery in a wide variety of industries are highly dependent on proper lubrication. As lubricant oil degrades through use, it gradually loses lubrication functionality, which results in damage to a machine [1]. More importantly a sudden change of lubricant properties may cause catastrophic machine failure [2]. While certain machines recommend interval-based oil changes (e.g., after a set number of miles in a car) to maintain desired machine performance, this estimative approach can be expensive, or cause damage to large machines such as wind turbines, reciprocating compressors, and CNC machines [3–5]. Online oil condition monitoring can detect multiple oil properties, predict the remaining life of the lubricant, determine the optimal oil change intervals, and avoid pending machine failures, thus significantly reducing the maintenance cost.

Viscosity is the leading parameter in indicating a lubricant's functionality and longevity [6,7]. To date, many sensors were developed, including micro machined cantilever sensors [8], acoustic sensors [9], and ratiometric fluorescent sensors [10] for online detection of viscosity. While viscosity can be measured independently, the change in viscosity could be caused by other oil property change (such as contents of acid, base and water); monitoring these properties could help identify the causes of lubricant degradation or possible machine failure [11]. Acid content is one of these properties that can give insight towards the degradation of an oil. Acidic byproducts are formed from oil oxidation, one of the primary causes for oil degradation and unwanted increases in viscosity [12]. Thus monitoring of acid content can provide information on the oxidation process [13]. Acid number increases of around 0.3 mg KOH/g are considered alarming for industrial lubricants. [14]. Similarly, many lubricant oils contain a base additive to neutralize these acid byproducts and slow the oxidation process, and as this base reserve depletes, the rate of oxidation will increase [15]. By comparing the trends of the base content with that of the acid content, a more complete picture of oil's remaining useful life can be generated, and concern should be raised when base levels deplete to lower than 2 mg KOH/g [16]. Water content is another important property to consider monitoring, as its presence in a lubricant oil can increase oxidation rates and cause rust and corrosion of machine surfaces [17]. Water content of 1000 ppm is considered to be an alarming amount [18].

While oil properties can be measured precisely in laboratories offline, the offline approach is time consuming and expensive considering the 1–2 week shipping and analysis time. Online monitoring of these key properties enables optimal oil change intervals and avoid sudden machine failure. Researchers have worked on sensors to monitor individual oil properties online. Agoston et al. [6] were able to evaluate the oil characteristics associated with oxidation using a micro acoustic sensor; however, the sensor was not able to detect bulk changes caused by additives found in lubricant oils. Several groups have utilized electrochemical sensors to measure TAN/TBN of oil samples [19,20]. The problem is that these sensors relied on chemical reactions between the sensing materials and contents of oils, which greatly shorten the lifespan of the sensor, making them unsuitable for prolonged and continuous measurements. Li [21] developed a micro sensor array with individual sensors that determined acid and water content. Since this array

* Corresponding author.
E-mail address: jzhe@uakron.edu (J. Zhe).

https://doi.org/10.1016/j.triboint.2021.107221
Received 15 April 2021; Received in revised form 15 July 2021; Accepted 2 August 2021
Available online 5 August 2021

correlated the raw data of the sensor to various properties, it required detailed information such as oil formulation, viscosity, and dielectric constant in order to evaluate the lubricant's status [21]. Smiechowski et al. [20,22] also developed electrochemical sensor array to detect multiple oil properties. Due to the long standing cross sensitivity problem of electrochemical sensors, i.e, each sensor not only responds to the target property but other properties in the oil as well, the sensor array has difficulty in providing accurate TAN/TBN predictions.

Artificial neural networks (ANNs) are computing systems that have been proven effective in processing sensors with overlapping responses. Back propagation artificial neural networks (BPNNs) have been used by various groups in determining CO and CH_4 in mixtures [23], analyzing soil ions [24], classifying wines [25], monitoring water quality [26], and monitoring tool conditions [27]. Zhu et al. [28] applied an BPNN to a sensor array to predict acid, water, soot, and sulfur content in lubricant oil. While this system showed certain success in predicting oil properties from overlapped sensor responses, the training process for BPNNs is complex and tedious [29]; a large amount of training data set is required in order to establish the BPNN, and gathering sufficient training data set could be lengthy, costly, and complex [30].

A general regression neural network (GRNN) is an artificial neural network that utilizes a single pass algorithm, which can offer certain advantages when compared with back propagation neural networks (BPNNs). Radial basis Function and Elman neural network can provide decent predictions but typically require a large data set [31,32]. GRNNs have the ability to generate accurate predictions with smaller data sets [30], which is an essential feature when data is not readily available and tedious to generate. GRNNs also offer the ability to expand a data set without reestablishing the network since they operate with a single forward pass algorithm [33]. In comparison, to expand a data set for a BPNN, the entire network must be completely retrained [34]. GRNNs have seen utility in predicting wind speeds [35], steel properties after thermomechanical processing [36], and the performance and exhaust characteristics of combustion engines [37]. With these advantages, in this article, we will establish a GRNN on a sensor array to detect the levels of multiple properties that are critical to the functionality of industrial lubricant oil. By implementing a GRNN to our sensor array, we are able to simplify training procedures while accurately and continuously monitor the contents of acid, base and water in lubricant oils. To our knowledge, this is the first work that had utilized the GRNN in online oil condition monitoring.

2. Materials and method

We designed an array of 3 capacitive sensors for measuring acid, base, and water contents. The capacitive sensors have similar designs but have different absorbent coatings. The specific coating ensures that each sensor is more sensitive to one property than other properties, so that each sensor will respond to different properties with different weights. Fig. 1A and B illustrate the side and top view of the capacitive sensors. Since there are still certain cross sensitivities, the responses are sent through a GRNN to decipher the overlapping responses from the sensor array.

All 3 sensors capacitive sensors utilize interdigitated electrodes (IDEs) to form capacitors. Changes in the capacitance can be attributed to dielectric changes of the medium (e.g. lubricant oil) between the fingers. Unique coatings were applied to the IDEs to make sensors respond to properties differently from each other. Fig. 2 shows a magnified image of the IDE electrodes.

Each sensor was fabricated using standard photolithography processes followed by a spin coating. The IDEs of the three capacitive sensors had the same geometry. The IDE electrodes were fabricated on a glass substrate with a 100 nm gold layer, and a 5 nm titanium adhesion layer (EMF Corporation, TA134). The IDE pattern had 40 pairs of fingers, each with a length of 5 mm. The width (W) of the fingers was designed to 25 μm, while the gap (G) between them was 50 μm (see Fig. 1B). The IDE capacitive sensors were all coated with absorbent materials with appropriate thickness to provide varying sensitivities to different properties. Sensor 1 is designed to have an increased response to water, the IDEs were coated with a layer of polyimide, a material that absorbs water [38,39] but rejects lubricant oil. The thickness of the polyimide coating was measured to be approximately 4 μm. Note that the strength of the electric field can be neglected beyond a vertical distance of

$$\lambda = (W + G) \tag{1}$$

where λ represents the vertical distance from the IDE surface, W represents the finger width, and G represents the finger gap (as shown in Fig. 1). Changes of the medium beyond that distance have no effect on the sensor response [40]. Thus sensor 1 primarily responds to the water content but also responds to other oil property change (e.g. acid, base contents).

Sensor 2 was coated with a layer of polytetrafluoroethylene (PTFE), a hydrophobic material that resists the absorption of water. A PTFE (Teflon) tape was applied over the IDEs with a thickness of 70 μm,

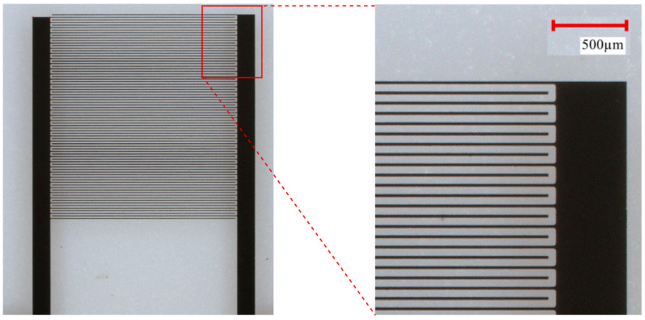

Fig. 2. Microscopic picture of Interdigital electrodes of the capacitive sensor.

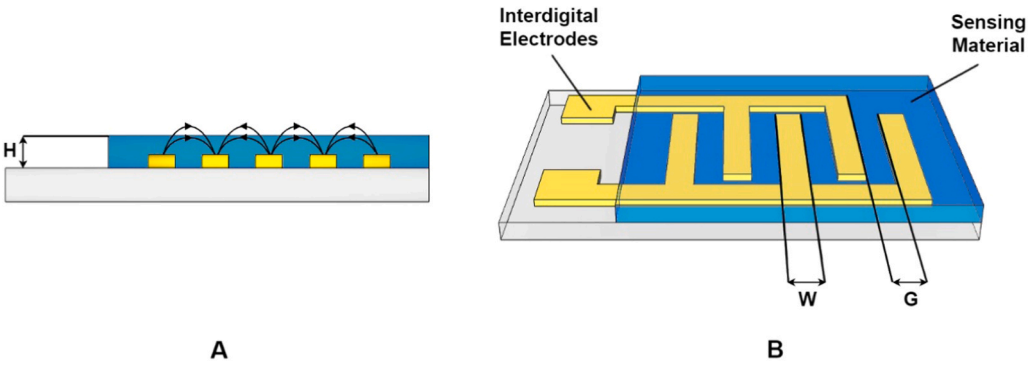

Fig. 1. A) Side view of capacitive sensors with interdigital electrodes, B) Top-down view describing the capacitive sensor's structure.

within λ/2. Therefore this sensor will respond to all property changes in the oil, while remaining largely indifferent to changes of water content within the oil [41].

Sensor 3 was coated with Nafion, a material commonly used as a cation exchange membrane due to its ability to allow the passage of positively charged ions [42]. A Nafion (Alfa Aesar, Nafion D-521 dispersion) film of ~250 nm was spin coated on The IDE surface. Sensor 3 primarily responds to acid and base, different from Sensors 1 and 2.

3. Theory

We utilize a General Regression Neural Network (GRNN) to remove the cross sensitivities of the responses from the sensor array. The GRNN was developed in MatLab, and consists of an input layer, a radial basis layer, a linear layer, and an output layer as shown in Fig. 3. Each node (or neuron) in the input layer represents the relative voltage/capacitance change from one sensor, while each neuron in the output layer represents the corresponding acid/base/water content to be determined. The number of neurons in the radial basis layer is equal to the number of sample data points used to create the network. Each neuron in the hidden layer is related to all the neurons in the previous layer via a distance value that is passed through a radial basis function (see Fig. 3). When predicting the oil properties, we will first find the Euclidean distance between the inputs for this data point and the inputs of the whole dataset. The Euclidean distance is defined as follows:

$$Euclidean\ Distance = \sqrt{\sum_{i=1}^{n}(x_i - y_i)} \tag{2}$$

where x_i is the data point's input from the i^{th}sensor, y_i is the input from i^{th}sensor of a single entry in the GRNN dataset, and n is the number of inputs in the network. This distance is calculated for every entry in the dataset, and this array is multiplied by a scalar bias. This bias is defined as follows:

$$Bias = \frac{\sqrt{-\ln 0.5}}{\sigma} \tag{3}$$

where σ is the smoothing factor, a parameter that affects smoothness of the network's prediction curve as well as its ability to generalize. We determined an optimal smoothing factor for our network through an iterative process; the process is discussed in section. Each value of the array resulting from multiplying the bias and the distance is passed through a radial basis function, defined as follows:

$$RadialBasis(n) = e^{-n^2} \tag{4}$$

where n represents the values of the array resulting from the previous step.

Finally, a normalized dot product between this resulting array and the outputs of the GRNN's data set giving the predicted values, as follows:

$$rediction = \frac{A \cdot Z}{\sum_i^d Z_i} \tag{5}$$

where A is the array of outputs in the GRNN's dataset, Z is the array generated from the previous step, and d is the number of data points in the GRNN's dataset.

Because the GRNN uses forward propagation, it has several advantages compared to a BPNN. To expand the dataset in a BPNN, the network needs to be completely retrained, and weights need to be reassigned between every node. For a GRNN, the dataset can simply be expanded with new samples without requiring a new training procedure [43]. This convenience allows for the network to be tailored to a user's requirements easily. Prior research also demonstrated that the GRNN displayed better accuracy when sample sizes are not very large [43,44].

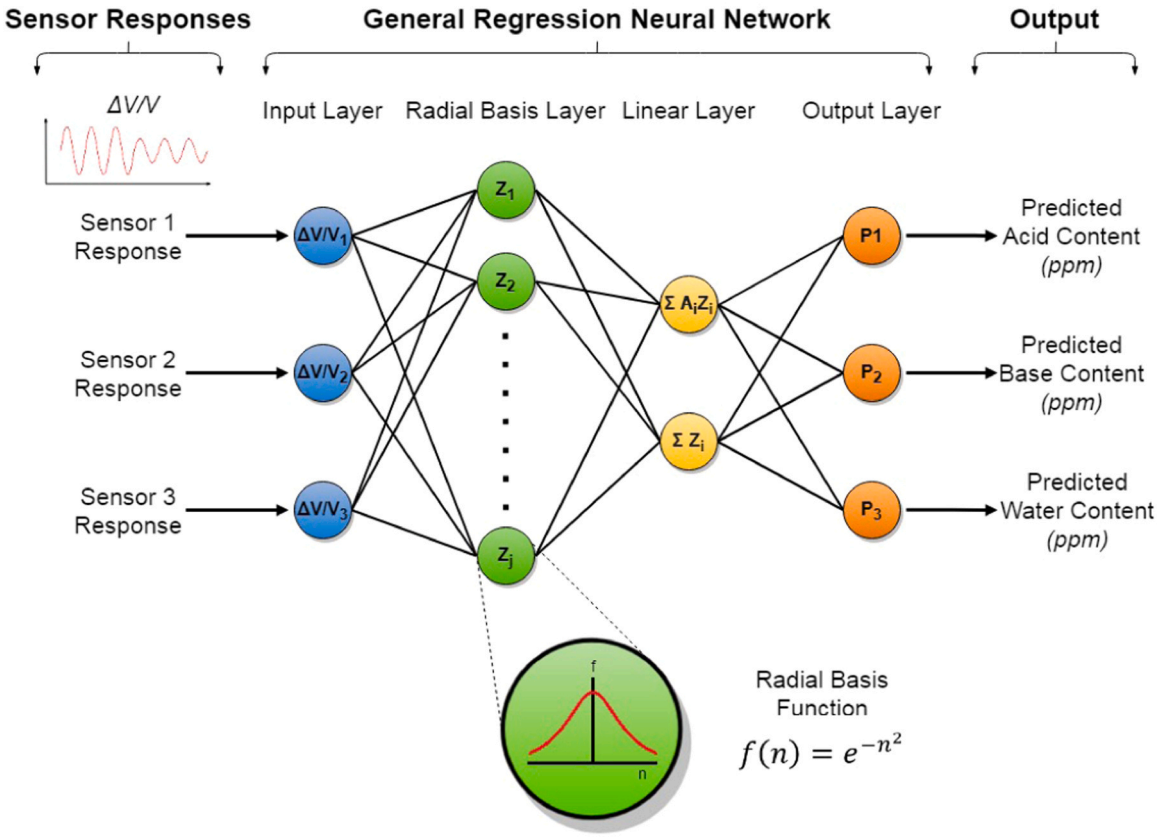

Fig. 3. Illustration of the GRNN architecture for oil condition monitoring.

Because it is impractical to generate huge datasets online, the GRNN is more suitable for online oil condition monitoring.

Next, we prepared 48 oil samples, 36 were used for training to determine an optimal smoothing factor, and 12 were used as a final testing dataset. These samples contained varying concentrations of acid, base, and water. Water contents were altered by adding H_2O at concentrations of 500, 1000, and 1500 ppm. Sulfuric acid (H_2SO_4) and potassium hydroxide (KOH) were used to change the receptive acid and base levels at concentrations of 1000, 2000, 3000, and 4000 ppm. Conventional oil (MAG1, Conventional 10W30) was used as a base oil. These concentrations were chosen to simulate conditions that have been used by industrial lubrication systems [14,16,18,45]. Individual samples were prepared and thoroughly mixed right before testing to prevent any separation. Samples were loaded into a tank; the 3 capacitive sensors were installed on the side wall of the tank (see Fig. 4). Oil was circulated via a pump at a fixed flow rate of 100 mL/min. The excitation signal for the sensors array was a 2 MHz, 10 V_{pp} sine wave via a function generator (Agilent, 33,600 A Series). Sensor responses were recorded through the DAQ device (NI, PCI-6133) after 20 min, and sensors were cleaned and dried between testing with different samples. Changes in the concentrations of various properties in the oil leads to changes in the capacitance of the IDE sensors. This capacitance change correlates with an impedance change of the sensor. To measure this change, voltages across the capacitive sensors were recorded with a DAQ (see Fig. 4). To reduce the amount of data, an under-sampling technique was used to capture voltage peaks, which significantly reduced the amount of the collected data. With this reduced amount of data, the device is more suitable for online oil condition monitoring. Details of under sampling method can be found in our prior publication [46]. With the under sampling, we were able to use a sampling rate of 110 kHz to capture the peaks of a 2 MHz sine wave signal.

After the raw data was collected, a fast Fourier transform (FFT) was applied to filter out unwanted noises. The average peak voltage was calculated, and was imported to the GRNN (see Fig. 3) to calculate the target properties. The GRNN was developed in MatLab using built-in neural network tools and custom code for analysis. The network contains an input layer, a radial basis layer, a pattern layer, and an output layer. The input and output layers have 3 nodes, corresponding to the number of sensors and number of properties. The radial basis layer contains 32 nodes, corresponding to the number of training samples, and the linear layer has 2 nodes.

4. Results and discussion

For the GRNN to make accurate predictions, it is critical that the sensor response to each property has a good trend. To test this, we measured the sensors' responses to samples with changes in only one property. For each oil sample, the measurements of sensors' responses were taken at t = 20 min after submersion of the sensors. Before the sensors were tested in the next oil sample, the sensors were cleaned and dried. Sensors' responses to oil samples with varying contents of only one property (water, acid, or base) were plotted in Fig. 5. Each error bar represents standard deviation of three separate measurements of one sample.

The collected data met this criteria, as the relative voltage change for acid steadily increased from −0.15% to −0.04% (Teflon coated sensor), decreased from −0.2% to −20.9% for base (Nafion coated sensor), and decreased from −0.2 to −0.27 for water (Polyimide coated sensor), as shown in Fig. 5. Next, the sensors were measured with the 36 training oil samples to train the network and an additional 12 testing samples to evaluate the accuracy of the network. These 48 samples contain different combinations of acid, base, and water contents discussed in the previous section. The sensor responses were collected when they were submerged in the oil sample for 20 min. (Typical time series sensor responses are given in the Supplement materials). During network training, the training dataset of 36 was randomly divided into 5 groups. A k-fold cross validation method was used on these groups: 4 groups were used for training, while the remaining group was used for validation in determining the optimal smoothing factor. This process was repeated 4 more times until each group was used as the validation group. After training, the network was tested on the separate testing dataset (12 samples) to determine the networks performance on data it was not trained with.

During training, the network was run for a range of smoothing factors from 0.0001 to.5 in steps of.00001 in order to determine the optimal value. All errors were normalized to have even weight since the monitored ppm range for the properties were different, and the smoothing factor with the lowest combined normalized error was selected for our network. Data was normalized by multiplying the water error (ppm) by a value of 4000/1500 to account for the difference in range from water to acid/base content. One focus of this study is to reduce the amount of training samples while keeping satisfactory accuracy, because using a large number of samples for training is impracticable for onsite oil property monitoring. We conducted the training using various sizes of training samples (20, 26, and 36). Results are shown in Fig. 6. As shown in Fig. 6, the difference between using the three training samples sizes is negligible. The optimal smoothing factor for the GRNN was found to be.0150, 0.0153 and 0.0158 respectively. We used 0.0150 for the subsequent predictions with the 20 sample dataset in Fig. 8.

Since data can be iteratively added to the GRNN without a retraining process, we were able to monitor the trend of the network's prediction error as samples were added to the dataset. By analyzing the average prediction error for each property, we could add samples to whichever property had the highest error to further reduce that error. The average prediction error was calculated by taking the average of the percent errors from each prediction from the test group, as shown in Eq. (6).

$$Average\ Prediction\ Error = \frac{\sum E_{test}}{n_{test}} \tag{6}$$

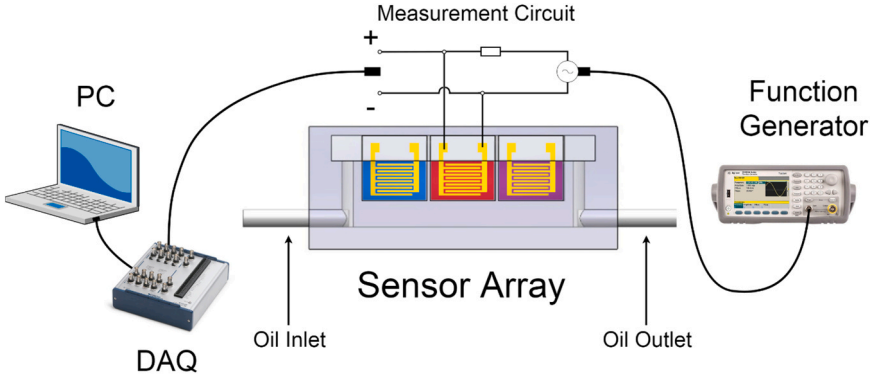

Fig. 4. Experimental setup for the sensor array for oil condition monitoring.

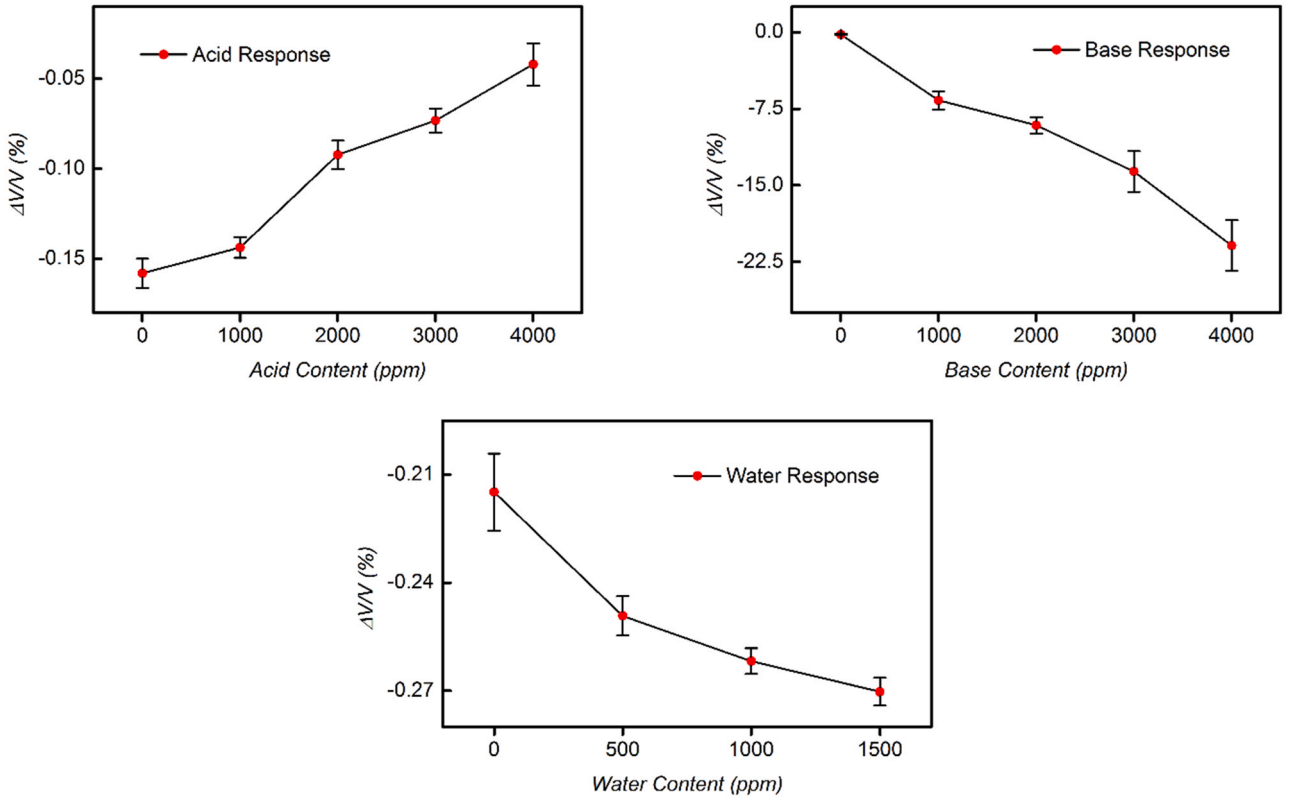

Fig. 5. Raw Sensor Responses to oil samples with varying contents of only one property (water, acid, or base). (a): Relative voltage change of Teflon coated sensor to oil samples with varying acid content. (b): Relative voltage change of Nafion coated sensor to oil samples with varying base content. (c): Relative voltage change of Polyimide sensor to oil samples with varying water content.

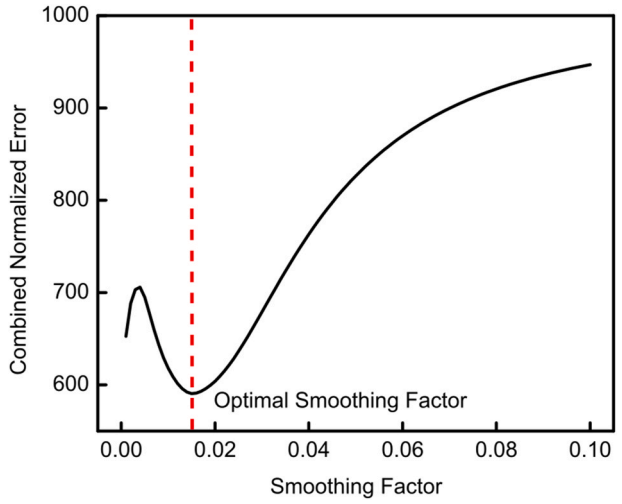

Fig. 6. Smoothing factor vs. normalized combined error of all 3 properties with different amount of training samples, 20, 26 and 36.

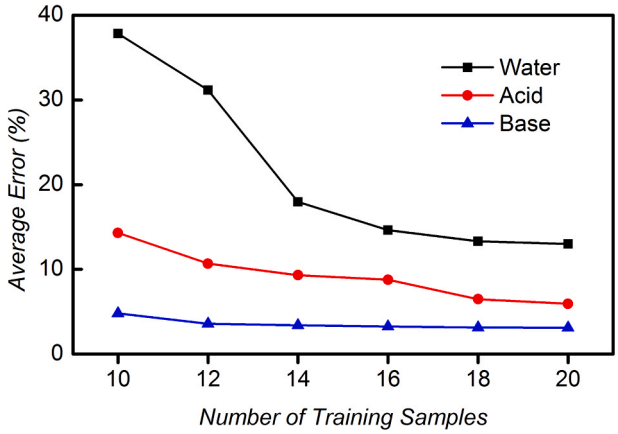

Fig. 7. Average prediction error versus various sizes of training dataset. (a) gathered from 36 training samples, (b) gathered from 12 testing samples.

where E_{test} is the percent error for a single prediction from the test dataset, and n_{test} is the number of datapoints in the test dataset. Fig. 7a shows the average prediction error collected from the 36 training samples. It is obvious that the average prediction errors only decreased a little when the training samples was increased from 20 to 36.

Finally, the network was tested using samples with various concentration of the acid, base and water. The samples cover a wide range of property contents, acid from 0 to 4000 ppm, base from 0 to 4000 ppm, and water from 0 to 1500 ppm. These ranges cover critical areas for lubricant functionality in industrial machinery [14,16,18]. Fig. 7b shows the average prediction error collected from 12 testing samples when the network was trained with different samples sizes. As we increased training dataset from 10 to 20, the average water content error was reduced from 38% to 13%, the average acid error from 14% to 6%, and the average base error from 5% to 3% (see Fig. 7B). We found a 20-sample training dataset was sufficient. Additional samples only decreased the average prediction error by a small amount. When the dataset was increased from 20 to 36 samples, the error reduction for acid, base, and water content were only.72%,.05%, and 1.8% respectively.

Fig. 8 shows the predicted contents by the GRNN were compared to

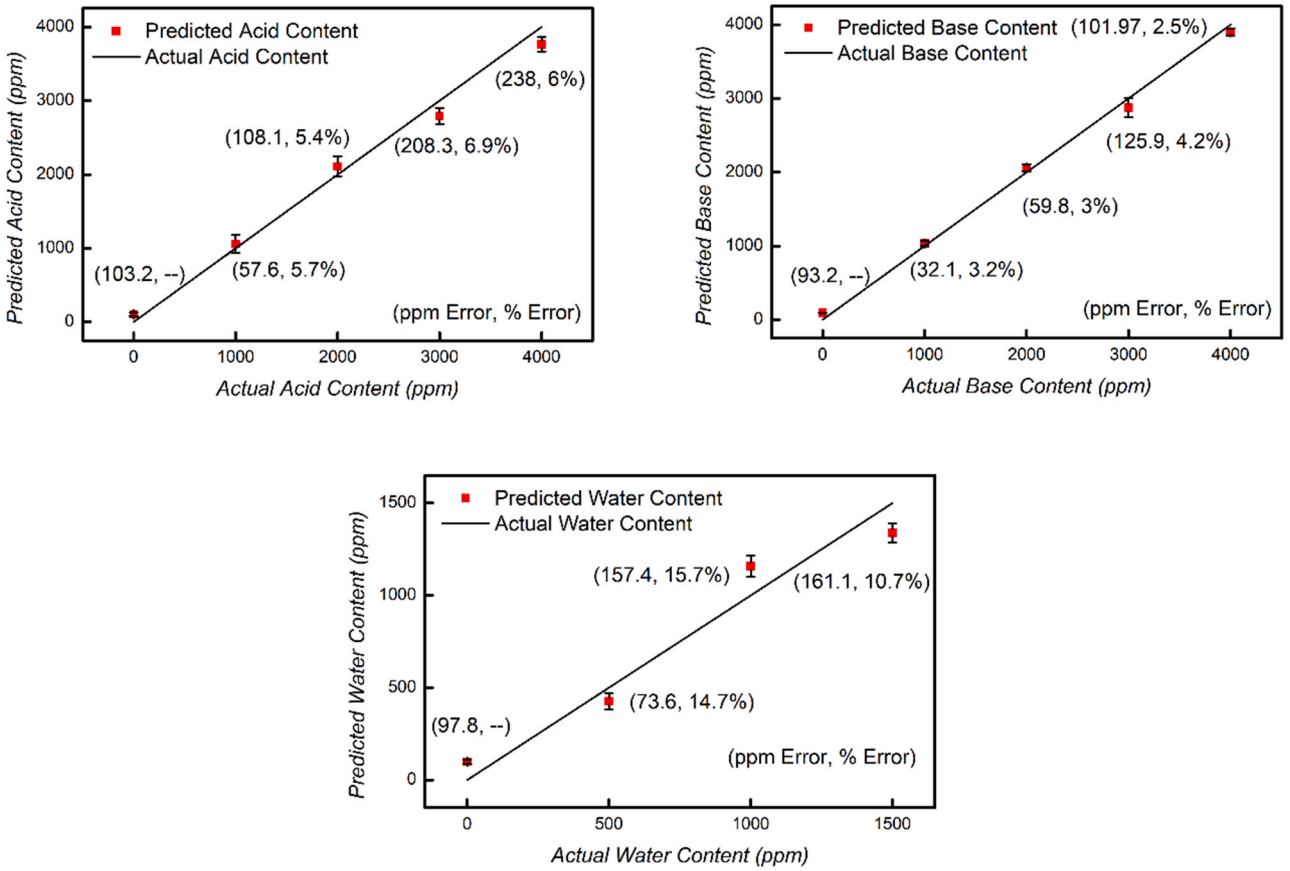

Fig. 8. Testing data errors (a): Actual vs. predicted values for acid content (b): Actual vs. predicted values for base content (c): Water vs. predicted values for water content.

the actual contents for the 12 testing samples, which were not used in training. Each sample was measured 3 times with an interval of 2 h. As shown in Fig. 8, the two sets of values are in good agreement. The maximum percent error for acid, base, and water content was 6.9%, 4.2%, and 15.7% respectively. The comparatively higher prediction error in water content can be attributed to the fact that changes in water content had the smallest corresponding sensor responses in magnitude. This effect is also evident for the base predictions, where the highest sensor response resulted in the smallest error. Based on these results, this sensor array in combination with the GRNN is capable of untangling non-linear and overlapped sensor responses and making accurate predictions of multiple properties of a lubricant oil.

The prediction error of this system can be reduced by two approaches. First, the noise from the raw signal, especially for the sensor which had a lower sensitivity is one of the major sources for the prediction errors. For example, the prediction in water content has a larger average error (14%) than the other properties (6% and 3%). This is because the Teflon coated sensor has a low sensitivity to water content change; therefore, the relative amplitude of the noise is larger than that of the other properties. The prediction error can be reduced by using a coating material that generates higher sensitivity to the target property. We also found that reducing the thickness of the sensing material would increase the sensitivity, although the measurement range of the sensor is reduced. Further analysis on selecting the optimal sensing layer thickness could provide greater sensitivity while maintaining a range that covers the critical points. Second, adding more training samples, especially at smaller concentration ranges, may potentially reduce the prediction error at the price of a longer training time.

To provide comparison with other networks, we established two additional neural networks, a radial basis network and a back propagation neural network, to make predictions and determined their respective errors. Both of these networks were established using MatLab's neural network toolbox. The radial basis network has a similar first layer to the GRNN, but has a different linear layer [47]. This network gave maximum error predictions of 8.1%, 4.4%, and 18.8% for acid, base, and water contents respectively. The back propagation neural network (BPNN) contained 2 layers, with 42 nodes in the first layer and 4 nodes in the second layer. The network was trained using the Levenberg-Marquardt backpropagation algorithm. The maximum prediction errors during validation for this network were 12.5%, 4.9%, and 23.6% for acid, base, and water contents respectively. We also compared computational time in training. The computation for GRNN and radial basis networks were completed in 49 and 44 s respectively, while the BPNN took 433 s. This was expected, since the GRNN and radial basis networks only needed to sweep through smoothing factors, while the BPNN needed to reassign all weights among nodes over many iterations. When comparing the prediction errors, the GRNN showed superior performance across all three properties on our dataset.

It is worth mentioning here that we employed the fruit-fly optimization algorithm [48] and found it was able to find an optimal smoothing factor in 30 s. In comparison, the sweeping method (i.e. sweeping a large range of smoothing factors with a small step) took approximately 49 s. All calculations were performed in a Dell Latitude 5420 laptop. Nevertheless, the prediction accuracy was not affected as the smoothing factors obtained from the fruit-fly algorithm and the sweep method had negligible differences (0.0150 vs 0.01504). While the improvement in training time is limited because of the small amount of samples, we believe this algorithm can improve the training speed significantly in applications with a large number of training samples.

Since there could be unexpected contaminants in the lubricant oil that are not being measured by the system, it is important to make sure these contaminants would not have a large impact on the sensors. Wear

debris particle are the most common substances existing in the running lubricant. We tested the influence of the wear debris on the GRNN prediction by introducing iron and ceramic wear debris into the lubricant. A 30 ppm concentration of iron particles resulted in a.0038% voltage change, while a 40 ppm concentration of ceramic particles resulted in a.0069% voltage change. Such a change would result in approximately a 0.2% and 0.5% error from GRNN, which can be neglected. Note that the concentrations of wear debris were selected based on what would be expected in industrial applications [49].

The capacitive sensors' responses change are caused by the change in relative permittivity of the oil [40]. The permittivity change is not directly dependent on machine operating parameters such as rotational speed or torque, but is effected by the oil operating temperature [50]. Currently, data collection was done at the expected oil operating temperature. We plan to add a temperature sensor as an input in future works, as temperature variation could lead to less accurate predictions.

More sensors with other sensing materials can be added to or removed from the GRNN to detect additional/other properties. The GRNN can easily be modified to allow any number of sensor inputs and property outputs. As long as every property has a detectable trend from a sensor, the network can make accurate predictions after training. Additional sensors will not have a noticeable negative effect on current property predictions as long as they provide relevant data [51]. Furthermore, singular spectrum analysis can be coupled with the GRNN to further reduce unwanted noises and increase signal strength, demonstrated in wind-speed forecasting and industrial production forecasting applications [52,53]. This could further increase the sensitivity, and decrease prediction error.

We have developed a capacitive sensor array in combination with a GRNN to accurately measure multiple lubricant oil properties from overlapped sensor responses. Each of the three sensors in the array has a different response to changes in key lubricant properties: acid, base, and water content. The GRNN has displayed the ability to make accurate measurements of these properties with a small amount of training samples. The network was able to predict acid, base, and water content within errors of 6.9%, 4.2%, and 15.7% respectively. The system also displayed ability to function properly even with unexpected contaminants (e.g. wear debris) in the oil. Through use of the GRNN, we were able to simplify the training process without sacrificing the measurement accuracy. By monitoring the key oil properties, the remaining useful life of lubricant oil can be predicted to avoid catastrophic machine failure as well as unnecessary premature oil changes. In addition, while we demonstrated measurement of three oil properties, more sensors, including but not limited to, sensors who respond to soot, sulfur, or glycol contents, can be added to the sensor array to monitor additional oil properties and provide complete information on lubricant oil, and can be used for health monitoring of a variety of machines, including turbomachines, combustion engines and heavy equipment.

Funding

This material is based upon work supported by the National Science Foundation of USA under grant numbers PFI-TT 1940879 and I-Corps 2027849. Any opinions, findings, and conclusions or recommendations expressed in this material are those of the author(s) and do not necessarily reflect the views of the National Science Foundation.

CRediT authorship contribution statement

Dian Jiao: Conceptualization, Software, Formal analysis, Investigation, Writing – original draft, Writing – review & editing. **Aaron Urban:** Conceptualization, Software, Formal analysis, Investigation, Writing – original draft, Writing – review & editing. **Xiaoliang Zhu:** Conceptualization. **Jiang Zhe:** Writing – review & editing, Supervision, Funding acquisition.

Declaration of Competing Interest

The authors declare that they have no known competing financial interests or personal relationships that could have appeared to influence the work reported in this paper.

Appendix A. Supporting information

Supplementary data associated with this article can be found in the online version at doi:10.1016/j.triboint.2021.107221.

References

[1] He, Q., Chen, G., Chen, X., Yao, C, Application of oil analysis to the condition monitoring of large engineering machinery. In Proceedings of the Proceedings of 2009 8th International Conference on Reliability, Maintainability and Safety, ICRMS 2009; 2009; pp. 1100–1103.
[2] Ku PM. Gear failure modes—importance of lubrication and mechanics. A S L E Trans 1976;19:239–49. https://doi.org/10.1080/05698197608982799.
[3] Fernandes CMCG, Martins RC, Seabra JHO. Friction torque of thrust ball bearings lubricated with wind turbine gear oils. Tribology Int 2013;58:47–54. https://doi.org/10.1016/j.triboint.2012.09.005.
[4] Ozsipahi M, Kose HA, Cadirci S, Kerpicci H, Gunes H. Experimental and numerical investigation of lubrication system for reciprocating compressor. Int J Refrig 2019; 108:224–33. https://doi.org/10.1016/j.ijrefrig.2019.08.026.
[5] Huang J, Tan J, Fang H, Gong F, Wang J. Tribological and wear performances of graphene-oil nanofluid under industrial high-speed rotation. Tribology Int 2019; 135:112–20. https://doi.org/10.1016/j.triboint.2019.02.041.
[6] Agoston A, Ötsch C, Jakoby B. Viscosity sensors for engine oil condition monitoring - application and interpretation of results. Sens Actuators A Phys 2005;121:327–32. https://doi.org/10.1016/j.sna.2005.02.024.
[7] Brouwer MD, Gupta LA, Sadeghi F, Peroulis D, Adams D. Femoral revision surgery with impaction bone grafting: 31 hips followed prospectively for ten to 15 years. J Bone Jt Surg Br Vol 2012;94. https://doi.org/10.1016/j.sna.2011.10.024.
[8] Agoston A, Keplinger F, Jakoby B. Evaluation of a vibrating micromachined cantilever sensor for measuring the viscosity of complex organic liquids. Sens Actuators A Phys 2005;123–124:82–6.
[9] Zhu X, Du L, Zhe J. An integrated lubricant oil conditioning sensor using signal multiplexing. J Micromech Microeng 2014;25:015006. https://doi.org/10.1088/0960-1317/25/1/015006.
[10] Haidekker MA, Brady TP, Lichlyter D, Theodorakis EA. A ratiometric fluorescent viscosity sensor. J Am Chem Soc 2006;128:398–9. https://doi.org/10.1021/ja056370a.
[11] Ahmad MA, Yahya WJ, Ithnin AM, Hasannuddin AK, Bakar M, Fatah A, et al. Performance, emissions and lubricant oil analysis of diesel engine running on emulsion fuel. Energy Convers Manag 2016;117:548–57. https://doi.org/10.1016/j.enconman.2016.03.057.
[12] Markova LV, Makarenko VM, Semenyuk MS, Zozulya AP. On-line monitoring of the viscosity of lubricating oils. J Frict Wear 2010;31:433–42. https://doi.org/10.3103/S106836661006005X.
[13] Coiclough T. Role of additives and transition metals in lubricating oil oxidation. Ind Eng Chem Res 1987;26:1888–95. https://doi.org/10.1021/ie00069a028.
[14] Richard Booser, E., Kauffman, R, Rapid Determination of Remaining Useful Lubricant Life. In CRC Handbook of Lubrication and Tribology, Volume III; 1993.
[15] Rudnick, L.R., Synthetics, mineral oils, and bio-based lubricants: Chemistry and technology; 2005; ISBN 9781420027181.
[16] Shubkin, R.L., Synthetic lubricants and high-performance functional fluids. 1993; doi:10.1016/0301–679x(94)90064–7.
[17] Cantley RE. The effect of water in lubricating oil on bearing fatigue life. ASLE Trans 1977;20:244–8. https://doi.org/10.1080/05698197708982838.
[18] Foster NS, Amonette JE, Autrey T, Ho JT. Detection of trace levels of water in oil by photoacoustic spectroscopy. Sens Actuators B Chem 2001;77:620–4. https://doi.org/10.1016/S0925-4005(01)00767-5.
[19] Moon S, Il, Paek KK, Lee YH, Kim JK, Kim SW, et al. Adjunctive rufinamide in Lennox-Gastaut syndrome: a long-term, open-label extension study. Acta Neurol Scand 2010;122. https://doi.org/10.1149/1.2209433.
[20] Smiechowski MF, Lvovich VF. Iridium oxide sensors for acidity and basicity detection in industrial lubricants. Sens Actuators B Chem 2003;96:261–7. https://doi.org/10.1016/S0925-4005(03)00542-2.
[21] Jingkun L., Development of a microfabricated sensor array for oil evaulation Jingkun Li Dr Diss 2005; 1, 158.
[22] Smiechowski MF, Lvovich VF. Electrochemical detection and characterization of proteins. Biosens Bioelectron 2006;22. https://doi.org/10.1016/S0022-0728(02)01106-3.
[23] Capone S, Siciliano P, Bârsan N, Weimar U, Vasanelli L. Analysis of CO and CH4 gas mixtures by using a micromachined sensor array. Sens Actuators B Chem 2001; 78:40–8. https://doi.org/10.1016/S0925-4005(01)00789-4.
[24] Wilson D, Gutiérrez JM, Alegret S, DelValle M. Simultaneous determination of Zn (II), Cu(II), Cd(II) and Pb(II) in soil samples employing an array of potentiometric sensors and an artificial neural network model. Electroanalysis 2012;24:2249–56. https://doi.org/10.1002/elan.201200440.

[25] Simões Da Costa AM, Delgadillo I, Rudnitskaya A. Detection of copper, lead, cadmium and iron in wine using electronic tongue sensor system. Talanta 2014; 129:63–71. https://doi.org/10.1016/j.talanta.2014.04.030.
[26] O'Connor E, Smeaton AF, O'Connor NE, Regan F. A neural network approach to smarter sensor networks for water quality monitoring. Sensors 2012;12:4605–32. https://doi.org/10.3390/s120404605.
[27] Dornfeld DA, DeVries MF. Neural network sensor fusion for tool condition monitoring. CIRP Ann Manuf Technol 1990;39:101–5. https://doi.org/10.1016/S0007-8506(07)61012-9.
[28] Zhu X, Du L, Liu B, Zhe J. A microsensor array for quantification of lubricant contaminants using a back propagation artificial neural network. J Micromech Microeng 2016;26:065005. https://doi.org/10.1088/0960-1317/26/6/065005.
[29] Wang J, Wu W, Zurada JM. Computational properties and convergence analysis of BPNN for cyclic and almost cyclic learning with penalty. Neural Netw J Int Neural Netw Soc 2012;33. https://doi.org/10.1016/j.neunet.2012.04.013.
[30] Dai Y, Guo J, Yang L, You W. A new approach of intelligent physical health evaluation based on GRNN and BPNN by using a wearable smart bracelet system. Proc Computer Sci. 2019:519–27.
[31] Zhang W, Qu Z, Zhang K, Mao W, Ma Y, Fan X. A combined model based on CEEMDAN and modified flower pollination algorithm for wind speed forecasting. Energy Convers Manag 2017;136:439–51. https://doi.org/10.1016/j.enconman.2017.01.022.
[32] Dantas TM, Cyrino Oliveira FL. Improving time series forecasting: an approach combining bootstrap aggregation, clusters and exponential smoothing. Int J Forecast 2018;34:748–91. https://doi.org/10.1016/j.ijforecast.2018.05.006.
[33] Hyndman RJ, Khandakar Y. Automatic time series forecasting: the forecast package for R. J Stat Softw 2008;11506:198–209. https://doi.org/10.18637/jss.v027.i03.
[34] Dai H, MacBeth C. Application of back-propagation neural networks to identification of seismic arrival types. Phys Earth Planet Inter 1997;101:177–88. https://doi.org/10.1016/S0031-9201(97)00004-6.
[35] Gao, S., Tian, J., Wang, F., Bai, Y., Yang, Q, The Study of GRNN for Wind Speed Forecasting Based on Markov Chain. In Proceedings of the 2015 International Conference on Modeling, Simulation and Applied Mathematics; Atlantic Press, 2015.
[36] Qiao L, Wang Z, Zhu J. Application of improved GRNN model to predict interlamellar spacing and mechanical properties of hypereutectoid steel. Mater Sci Eng A 2020;792:139845. https://doi.org/10.1016/j.msea.2020.139845.
[37] Bendu H, Deepak BBVL, Murugan S. Application of GRNN for the prediction of performance and exhaust emissions in HCCI engine using ethanol. Energy Convers Manag 2016;122:165–73. https://doi.org/10.1016/j.enconman.2016.05.061.
[38] Kang U, Wise KD. A novel method to detect functional microrna regulatory modules by bicliques merging. IEEE/ACM Trans Comput Biol Bioinforma 2016;13. https://doi.org/10.1109/16.830983.
[39] Laconte, J., Wilmart, V., Flandre, D., Raskin, J.P, High-Sensitivity Capacitive Humidity Sensor Using 3-Layer Patterned Polyimide Sensing Film. In Proceedings of the Proceedings of IEEE Sensors; 2003; p. 372.
[40] Hu X, Yang W. Planar capacitive sensors - designs and applications. Sens Rev 2010; 30:24–39. https://doi.org/10.1108/02602281011010772.
[41] Zhu H, Wang H, Wang F, Guo Y, Zhang H, Chen J. Preparation and properties of PTFE hollow fiber membranes for desalination through vacuum membrane distillation. J Memb Sci 2013;466:145–53. https://doi.org/10.1016/j.memsci.2013.06.037.
[42] Avci AH, Messana DA, Santoro S, Tufa RA, Curcio E, Di Profio G, et al. Energy harvesting from brines by reverse electrodialysis using nafion membranes. Membranes 2020:168. https://doi.org/10.3390/membranes10080168.
[43] Specht DF. A general regression neural network. IEEE Trans Neural Netw 1991;2: 568–76. https://doi.org/10.1109/72.97934.
[44] Martínez-Blanco M, del R, Ornelas-Vargas G, Solís-Sánchez LO, Castañeda-Miranada R, Vega-Carrillo HR, et al. A comparison of back propagation and generalized regression neural networks performance in neutron spectrometry. Appl Radiat Isot 2016;117:20–6. https://doi.org/10.1016/j.apradiso.2016.04.011.
[45] Booser, R., Twidale, A., Williams, D. Circulating Oil Systems. In CRC Handbook of Lubrication; 1988.
[46] Du L, Zhe J. Parallel sensing of metallic wear debris in lubricants using undersampling data processing. Tribol Int 2012;53:28–34. https://doi.org/10.1016/j.triboint.2012.04.005.
[47] Demuth, H., Beale, M. Neural Network Toolbox For Use with MATLAB. http://cda.psych.uiuc.edu/matlab_pdf/nnet.pdf (Accessed 24 May 2021).
[48] Xie X, Fu G, Xue Y, Zhao Z, Chen P, Lu B, et al. Risk prediction and factors risk analysis based on IFOA-GRNN and apriori algorithms: application of artificial intelligence in accident prevention. Process Saf Environ Prot 2019;122:169–84. https://doi.org/10.1016/j.psep.2018.11.019.
[49] Du L, Zhu X, Han Y, Zhao L, Zhe J. Improving sensitivity of an inductive pulse sensor for detection of metallic wear debris in lubricants using parallel LC resonance method. Meas Sci Technol 2013;24:075106. https://doi.org/10.1088/0957-0233/24/7/075106.
[50] Kaatze U. Complex permittivity of water as a function of frequency and temperature. J Chem Eng Data 1989;34:371–4. https://doi.org/10.1021/je00058a001.
[51] May, R., Dandy, G., Maier, H, Artificial Neural Networks: Methodological Advances and Biomedical Applications.
[52] Hassani H, Heravi S, Zhigljavsky A. Forecasting European industrial production with singular spectrum analysis. Int J Forecast 2009;25:103–18. https://doi.org/10.1016/j.ijforecast.2008.09.007.
[53] Wang J, Heng J, Xiao L, Wang C. Research and application of a combined model based on multi-objective optimization for multi-step ahead wind speed forecasting. Energy 2017;125:591–613. https://doi.org/10.1016/j.energy.2017.02.150.